Heat transfer during bubble formation

J. B. Haynes* and D. H. T. Gotham†

The flow around a gas bubble forming at a submerged orifice without vaporisation is analysed both with and without heat transfer taking place from the bubble surface. The results of experiments are given in which high-speed photography was used to study air bubbling through four different sizes of orifice into water, for the isothermal and diabatic case. A numerical solution of the dimensionless equations using Hamming's modified predictor–corrector method gave excellent agreement with experimental measurements of the bubble volume-time history for both stages of growth as well as predicting accurately the transition point between the two stages. Most of the heat transfer was found to occur almost immediately after the start of bubble growth

Key words: *Heat transfer, bubbles, orifices*

Gas discharging from an orifice into a liquid to form bubbles is a common feature in chemical engineering equipment. This report gives an account of a project to investigate the rate of heat transfer when high temperature gas bubbles are discharged into cold water.

Early attempts[1–4] to analyse the process of isothermal bubble formation, when both the gas and liquid have the same temperature, were based on a simple force balance on the bubble. More recently the velocity potential has been used[5–8] in an attempt to describe the flow around the forming bubble. McCann and Prince[6] assumed that, at any instant during the bubble formation period, the flow around the bubble could be described by a velocity potential which was only true for an expanding, translating sphere in an unbounded liquid. When the bubble is forming at an orifice plate, the presence of the plate affects the flow around the bubble and the velocity potential should be amended accordingly. Witze *et al*[7] obtained an approximate solution for the velocity potential about a growing bubble which took the presence of the orifice plate into consideration, although their analysis assumed that the bubble was completely spherical and rested tangentially on the plate throughout its entire formation period. However, when the bubble is connected to the orifice, initially it forms a truncated sphere. Kotake[8] derived the velocity potential for flow around a growing truncated sphere which allowed for the presence of the orifice plate.

The thermal behaviour of a vapour bubble during its formation has been the subject of a large number of investigations in the field of boiling. In these cases, heat transfer is accompanied by the mass transfer resulting from the phase change, so that the radial growth of the bubble can be related to the rate of heat transfer. For simple heat transfer this important relationship can no longer be used.

In one of the few publications dealing with heat transfer in the absence of mass transfer, L'Ecuyer and Murphy[9] obtained values for an average surface heat transfer coefficient during bubble formation which were based on the difference between bubble volume measurements made with and without heat transfer for the same experimental conditions.

Experimental studies have shown that there are four regions of bubble formation. One of these, the slowly increasing volume region, is the subject of this investigation.

Analysis

High-speed photography has shown that the bubble formation process can be divided into three stages which have been defined[5] as the growing stage, the elongating stage and the waiting stage. The analysis presented here deals with the first two of these stages.

The growing stage

The growing stage commences when the bubble is a hemisphere of radius equal to that of the orifice, and terminates when the forces acting on the bubble are in equilibrium. The motion of the bubble surface is considered as the superimposition of the radial velocity, $\dot{R}$, and the vertical translational velocity, $\dot{S}$. It can be seen from Fig 1 that for the base of the bubble to remain in contact with the orifice plate

$$\dot{S} = -\frac{\dot{R}}{\cos\theta^*} \tag{1}$$

where

$$\cos\theta^* = -\frac{S}{R} = \frac{-(R^2 - R_0^2)^{1/2}}{R} \tag{2}$$

By considering a control volume around the gas ante-chamber up to the edge of the orifice plate, and to a point in the gas supply where there exists

* Marcol Computer Services Ltd, formerly of the City University
† Department of Mechanical Engineering, The City University, Northampton Square, London, UK, EC1V 0HB

Received 31 March 1981 and accepted for publication 28 September 1981

a large pressure drop (eg sonic orifice), an expression for the mass flow rate through the orifice into the bubble is given by

$$\frac{dm}{dt} = \dot{W} - \frac{V_c}{\bar{R}T_c}\frac{dP_c}{dt} \tag{3}$$

Conservation of energy applied to the bubble for unsteady flow results in

$$\dot{Q} + C_p T_i \frac{dm}{dt} = C_v \frac{d(mT_b)}{dt} + P_b \frac{dV}{dt} + \sigma \frac{dA}{dt} + 3\mu_L \dot{S}^2 R\left(\tfrac{2}{3} - \cos\theta^* + \tfrac{1}{3}\cos^3\theta^*\right) \tag{4}$$

where the final three terms are associated with the work transfer due to the normal stress around the bubble surface, the surface tension, and the viscous effect.

The bubble volume, area and their respective rates of change are given by

$$V = \tfrac{2}{3}\pi R^3(1 - \cos\theta^* - \tfrac{1}{2}\cos\theta^* \sin^2\theta^*) \tag{5}$$

$$A = 2\pi R^2(1 - \cos\theta^*) \tag{6}$$

$$\frac{dV}{dt} = \frac{2}{3}\pi R^2 \frac{dR}{dt}\left(3 - 3\cos\theta^* - \frac{\sin^2\theta^*}{\cos\theta^*} - \frac{1}{2}\frac{\sin^4\theta^*}{\cos\theta^*} - \frac{1}{2}\sin\theta^*\cos\theta^*\right) \tag{7}$$

$$\frac{dA}{dt} = 2\pi R \frac{dR}{dt}\left(2 - 2\cos\theta^* - \frac{\sin^2\theta^*}{\cos\theta^*}\right) \tag{8}$$

Differentiation of the equation of state for an ideal gas yields

$$\frac{dP_b}{dt} = \left(\bar{R}T_b \frac{dm}{dt} + \bar{R}m\frac{dT_b}{dt} - P_b\frac{dV}{dt}\right)\frac{1}{V} \tag{9}$$

Differentiating Eqs (1) and (2) gives

$$\ddot{S} = -\frac{\ddot{R}}{\cos\theta^*} + \frac{\dot{R}^2}{R}\frac{\sin^2\theta^*}{\cos^3\theta^*} \tag{10}$$

The determination of the velocity potential for a growing bubble resting on a fixed plane boundary using the Laplace equation is complicated since the location of the plane boundary is a function of both r and θ. It has been shown[10] that by expressing Laplace's equation in terms of a toroidal coordinate system together with the appropriate boundary conditions gives the velocity potential as

$$\phi = 2R\left[(\dot{R} + \dot{S}\cos\eta_0) + \frac{\dot{S}\sin^2\eta_0}{(\cosh\omega\cos\eta_0)}\right] \times \left[\frac{(\cosh\omega + \cos\eta)}{(\cosh\omega + \cos\eta_0)}\right]^{1/2} \tag{11}$$

Using Bernoulli's equation to establish the pressure along a streamline around the bubble boundary, the mean pressure in the liquid around the bubble boundary is given by

$$\left[\frac{\bar{P}_L - P_\infty}{\rho_L}\right]_{r=R} = \dot{S}^2\left(\frac{\cos\theta^*}{2} - \frac{3}{2} + \frac{\cos^2\theta^*}{2}\right)$$

Nomenclature

A	Instantaneous bubble area
C_p	Specific heat of gas at constant pressure
C_v	Specific heat of gas at constant volume
F_{IB}	Force acting on bubble surface due to liquid inertia and buoyancy
F_μ	Viscous force acting on the bubble surface
F_σ	Surface tension force acting on the bubble surface
g	Gravitational acceleration
k	Thermal conductivity of the liquid
m	Instantaneous bubble mass
p_b	Instantaneous mean pressure of gas within the bubble
p_c	Instantaneous gas ante-chamber pressure
P_L	Liquid pressure
$\bar{P}_L$	Mean liquid pressure around the bubble surface
P_∞	Liquid pressure at the orifice in the absence of motion
$\dot{Q}$	Rate of heat transfer from the liquid to the bubble
r	Radial distance from centre of bubble
R	Instantaneous bubble radius
R_0	Orifice radius
$\bar{R}$	Gas constant
$\dot{R}$	Instantaneous radial velocity of bubble
$\ddot{R}$	Instantaneous radial acceleration of bubble
S	Instantaneous height of bubble centre above orifice
$\dot{S}$	Instantaneous translational velocity of bubble centre
$\ddot{S}$	Instantaneous translational acceleration of bubble centre
t	Time
T_b	Instantaneous mean bubble temperature
T_c	Temperature of gas in ante-chamber
T_i	Temperature of gas entering the orifice
T_L	Liquid temperature
T_∞	Bulk temperature of the liquid
T_p	Length of time period under consideration
V	Instantaneous bubble volume
V_c	Volume of gas ante-chamber
$\dot{W}$	Mean mass flow rate of gas into the ante-chamber
y	Radial displacement from bubble surface ($=r-R$)
α	Non-dimensional parameter ($=R/2S$)
α_t	Thermal diffusivity of liquid
β	Similarity variable ($y/\delta_t(\theta, t)$)
δ_t	Thermal boundary layer thickness ($=\delta_t(\theta, t)$)
Δp_μ	Increase in pressure across the bubble boundary due to viscosity
Δp_σ	Increase in pressure across the bubble boundary due to surface tension
ε	$=\delta_t^2$
η	Toroidal co-ordinate
η_0	Value of η on bubble surface
θ	Spherical co-ordinate
θ^*	Limiting angle of θ as shown in Fig 1
μ_L	Viscosity of liquid
ρ_L	Density of liquid
σ	Coefficient of surface tension
ϕ	Velocity potential
ω	Toroidal co-ordinate

$$+\dot{R}\dot{S}\left(\frac{8}{3}\cos\theta^*+\frac{2}{3}-\frac{7}{3\cos\theta^*}\right)$$
$$+\dot{R}^2\left(2-\frac{1}{2\cos\theta^*}\right)+2R\ddot{R}$$
$$+R\ddot{S}(\cos\theta^*+1)+g\frac{R}{2}(\cos\theta^*-1) \quad (12)$$

where

$$[\bar{P}_L]_{r=R}=\left[\frac{\iint_{\text{bubble surface}} P_L\,dA}{\iint_{\text{bubble surface}} dA}\right]_{r=R}$$

The mean pressure in the liquid around the bubble surface from energy considerations, $\bar{P}_L$, given by Eq (12) may be used to obtain the instantaneous mean pressure of the gas in the bubble, P_b, if the increase in pressure along the gas–liquid interface due to surface tension and viscosity of the liquid is included, ie

$$P_b-\bar{P}_L=\Delta P_\sigma+\Delta P_\mu \quad (13)$$

It has been shown[11] that the value of ΔP_μ may be given by

$$\Delta P_\mu=\frac{4\mu_L\dot{R}}{R} \quad (14)$$

while the value of ΔP_σ is given by[12]

$$\Delta P_\sigma=\frac{2\sigma}{R} \quad (15)$$

Eqs (1)–(10) and (12)–(15) enable the mean pressure of the gas in the bubble to be determined at every instant for the growing stage. The condition for the end of the growing stage is given by

$$F_{IB}-F_\sigma-F_\mu-\frac{(dm\dot{S})}{dt}=0 \quad (16)$$

where

$$F_{IB}=-2\pi R^2\left[\int_0^{\theta^*} P_L\sin\theta\cos\theta\,d\theta\right]_{r=R}$$
$$=2\pi R^2\rho_L\left[\dot{R}^2\left(\frac{11}{12}\cos^2\theta^*+\frac{1}{3\cos\theta^*}-\frac{5}{4}\right)\right.$$
$$+R\ddot{R}(\cos^2\theta^*-1)+\frac{2}{3}R\ddot{S}(\cos^3\theta^*-1)$$
$$+\dot{R}\dot{S}\left(\frac{17}{12}\cos^3\theta^*+\frac{5}{4\cos\theta^*}-2\cos\theta^*-\frac{2}{3}\right)$$
$$+\dot{S}^2\left(\frac{3}{8}\cos^4\theta^*+\frac{5}{8}-\cos^2\theta^*\right)-\frac{gS}{2}(\cos^2\theta^*-1)$$
$$\left.-\frac{gR}{3}(\cos^3\theta-1)+\frac{P_\infty}{2\rho_L}(\cos^2\theta^*-1)\right] \quad (17)$$

and

$$F_\sigma=2\pi R_0\sigma \quad (18)$$

$$F_\mu=4\pi\mu_L R\dot{S}\left[\frac{1-\cos\theta^*}{2}\right]^{1/2} \quad (19)$$

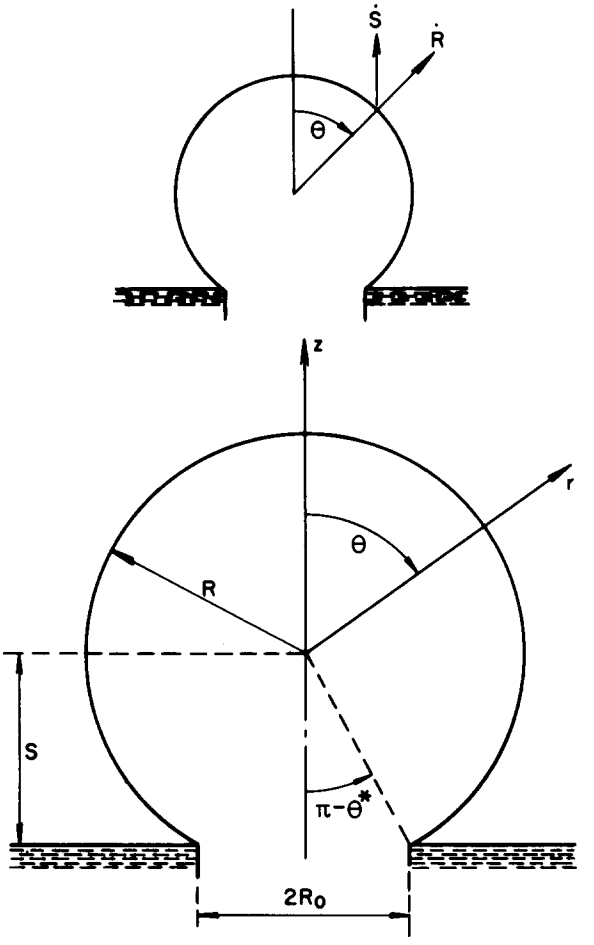

Fig 1 Bubble geometry and spherical co-ordinate system (growing stage)

Eqs (16)–(19) specify the end of the growing stage.

The elongating stage

The elongating stage commences when the net reactive force on the orifice plate becomes zero. During this stage, the bubble continues to grow and moves away from the orifice plate although the bubble remains connected to the orifice by a small neck. The elongating stage terminates when the neck of the bubble ruptures.

Assuming that the bubble is a complete sphere and that the bubble neck has negligible influence on the flow pattern, it has been shown[13,14], by use of the method of images, that the velocity potential for this case is given by

$$\phi=\left[\dot{R}\left(\frac{R^2}{r}+R\alpha+\frac{R}{2}\alpha^4+\frac{2}{3}R\alpha^6\right)-\dot{S}\left(\frac{R}{2}\alpha^2+\frac{R}{2}\alpha^5\right)\right]$$
$$+\left[\dot{S}\left(\frac{R^3}{2r^2}+\frac{R^3\alpha^3}{2r^2}+r\alpha^3+\frac{R^3\alpha^6}{2r^2}+r\alpha^6\right)\right.$$
$$\left.-\dot{R}\left(\frac{R^3}{2}\frac{\alpha^2}{r^2}+\frac{R^3\alpha^5}{2r^2}+r\alpha^2+r\alpha^5\right)\right]P_1(\cos\theta)$$
$$+\left[\dot{R}\left(\frac{2}{3}\frac{R^4}{r^3}\alpha^3+\frac{R^4}{r^3}\alpha^6+\frac{r^2}{R}\alpha^3+\frac{3}{2}\frac{r^2}{R}\alpha^6\right)\right.$$
$$\left.-\dot{S}\left(\frac{3}{2}\frac{r^2}{R}\alpha^4+\frac{R^4}{r^3}\alpha^4\right)\right]P_2(\cos\theta)$$

$$+\left[\dot{S}\left(2\frac{r^3}{R^2}\alpha^5+\frac{3}{2}\frac{R^5}{r^4}\alpha^5\right)\right.$$
$$\left.-\dot{R}\left(\frac{3}{4}\frac{R^5}{r^4}\alpha^4+\frac{r^3}{R^2}\alpha^4\right)\right]P_3(\cos\theta)$$
$$+\left[\dot{R}\left(\frac{4}{5}\frac{R^6}{r^5}\alpha^5+\frac{r^4}{R^3}\alpha^5\right)\right.$$
$$\left.-\dot{S}\left(2\frac{R^6}{r^5}\alpha^6+\frac{5}{2}\frac{r^4}{R^3}\alpha^6\right)\right]P_4(\cos\theta)$$
$$-\left[\dot{R}\left(\frac{5}{6}\frac{R^7}{r^6}\alpha^6+\frac{r^5}{R^4}\alpha^6\right)\right]P_5(\cos\theta) \qquad (20)$$

where $\alpha = R/2S$.

It should be noted that as $S\to\infty$ and hence $\alpha\to 0$ then Eq (20) reduces to

$$\phi = \frac{\dot{R}R^2}{r}+\frac{\dot{S}R^3}{2r^2}\cos\theta \qquad (21)$$

which is the velocity potential in the liquid around a growing bubble moving in an infinite medium, and has been used by several authors.[6,9].

In a similar manner to the growing stage theory, using Bernoulli's equation to evaluate a mean pressure in the liquid boundary around the bubble and superimposing the surface tension and viscous effects gives the pressure of the gas in the bubble as

$$\left[\frac{\bar{P}_L-P_\infty}{\rho_L}\right]_{r=R}$$
$$=R\ddot{R}\left[1+\alpha+\frac{\alpha^4}{2}+\frac{2}{3}\alpha^6\right]-R\ddot{S}\left[\frac{\alpha^2}{2}+\frac{\alpha^5}{2}\right]$$
$$+\dot{R}^2\left[\frac{3}{2}+2\alpha+\frac{7}{4}\alpha^4+3\alpha^6-\frac{3}{2}\alpha^7-\frac{21}{8}\alpha^8-5\alpha^9\right.$$
$$\left.-\frac{87}{20}\alpha^{10}-\frac{2705}{384}\alpha^{12}\right]$$
$$+\dot{S}^2\left[-\frac{1}{4}+\frac{\alpha^3}{2}+\frac{11}{4}\alpha^6-\frac{15}{4}\alpha^8-\frac{3}{2}\alpha^9\right.$$
$$\left.-\frac{21}{2}\alpha^{10}-\frac{93}{4}\alpha^{12}\right]-\dot{R}\dot{S}\left[2\alpha^2+4\alpha^5+3\alpha^7\right.$$
$$\left.-3\alpha^8-\frac{21}{2}\alpha^9-\frac{15}{2}\alpha^{10}-\frac{39}{2}\alpha^{11}\right]-gS \qquad (22)$$

Consideration of a force balance on the bubble surface[13] gives after some manipulation

$$2\pi R^2\rho_L[R\ddot{R}(\alpha^2+\alpha^5)-R\ddot{S}(\tfrac{1}{3}+\alpha^3+\alpha^6)$$
$$+\dot{S}^2(3\alpha^4+9\alpha^7-12\alpha^9-3\alpha^{10}-30\alpha^{11})$$
$$+\dot{R}^2(3\alpha^2+4\alpha^5-4\alpha^7-5\alpha^8-6\alpha^9-6\alpha^{10}-11\alpha^{11})$$
$$-\dot{R}\dot{S}(1+6\alpha^3+9\alpha^6-14\alpha^8-8\alpha^9-27\alpha^{10}-12\alpha^{11}$$
$$-23\alpha^{12})+\tfrac{2}{3}gR]-2\pi R_0\sigma-4\mu_L\pi R\dot{S}=\frac{d(m\dot{S})}{dt} \qquad (23)$$

Eqs (22), (23) and (3)–(9) with $\theta^*=\pi$ give a complete solution to the elongating stage.

Heat transfer

The rate of heat transfer between the bubble and the liquid with no mass transfer is given by

$$\dot{Q}=2\pi R^2k\int_0^{\theta^*}\left[\frac{\partial T_L}{\partial r}\right]_{r=R}\sin\theta\,d\theta \qquad (24)$$

Introducing the concept of a thermal boundary layer around the bubble whose thickness is a function of angular displacement and time and defining a similarity variable[15] defined by

$$\beta=\frac{\eta}{\delta_t(\theta,t)} \qquad (25)$$

to permit the solution of the diffusion equation gives

$$\frac{d^2T_L}{dt^2}+2\beta\frac{dT_L}{dt}=0 \qquad (26)$$

whose solution is given by

$$\frac{T_L-T_\infty}{T_b-T_\infty}=\operatorname{erfc}\left[\frac{y}{\delta_t(\theta,t)}\right] \qquad (27)$$

The rate of change of angular displacement for a fixed point in space is given by

$$\frac{3}{2}\frac{\dot{S}}{R}dt=\frac{d\theta}{\sin\theta} \qquad (28)$$

and

$$\frac{d\varepsilon}{dt}+\left(6\frac{\dot{S}}{R}\cos\theta+4\frac{\dot{R}}{R}\right)\varepsilon=4\alpha_t \qquad (29)$$

where $\varepsilon=\delta_t(\theta,t)^2$. Differentiation of Eq (27) gives

$$\left[\frac{dT_L}{dy}\right]_{y=0}=\frac{2}{\sqrt{\pi}}(T_\infty-T_b)\frac{1}{\delta_t(\theta,t)} \qquad (30)$$

and substituting (30) in (24) gives the rate of heat transfer between the bubble and the liquid as

$$\dot{Q}=4\sqrt{\pi}R^2k(T_\infty-T_b)\int_0^{\theta^*}\frac{\sin\theta}{\sqrt{\varepsilon}}d\theta \qquad (31)$$

Method of solution

In order to simplify the numerical solution and to avoid the possibility of rounding errors, the governing equations were expressed in dimensionless form[10].

Several numerical methods were used to determine their stability, relative accuracies and speed of execution.

The numerical method eventually chosen was Hamming's modified predictor–corrector method. A CDC 7600 computer was used to solve numerically the system of differential equations.

In order to obtain a complete solution, the value of the gas pressure in the ante-chamber, and its derivative, must be known for all time, t, during the bubble formation period. It was decided to use experimental values of the gas chamber pressure rather than employ the concept of an experimental discharge coefficient to determine the pressure drop across the orifice plate.

In order to solve the set of differential equations it was necessary to use a value for ε at

time $t = 0$. This initial value was determined by solving the diffusion equation in conjunction with the velocity potential for a liquid stream around a bubble translating through a medium at constant velocity.

Experimental investigation

The experimental equipment (Fig 2) consisted of a tank with an aluminium frame and ground glass sides, containing the liquid phase, mounted on top of a large metal cylinder. Air was injected into the liquid in the tank through a submerged aluminium orifice which was screwed into a Tufnel housing.

The orifice was supplied with air from a relatively small reservoir (gas ante-chamber) which fitted into the orifice housing and was surrounded by the metal cylinder. The air originated from a small compressor, and after passing through a series of filters, to dry and clean the air, entered a helical tube which was connected to the gas ante-chamber, and enclosed within the metal cylinder. Provision was made for preheating the air, prior to entry into the orifice, by immersing the helical tube in water contained in the cylinder which was kept at a constant temperature by means of electrical heaters. A controller was used to maintain a constant air mass flow rate into the ante-chamber which was measured by a calibrated rotameter. The temperature of the air entering the orifice was measured using a series of calibrated thermocouples.

A pressure transducer, connected to a flush mounted pressure tapping in the ante-chamber wall, was used to measure the pressure variation of the air in the ante-chamber. Because of the temperature limitation imposed on the pressure transducer, it was fitted outside the metal cylinder and connected to the pressure tapping by a short length of water cooled copper tubing. A UV (ultra-violet) recorder was used to obtain a trace of the output from the pressure transducer.

The bubble formation process was photographed with a Hycam high-speed camera using rear lighting to highlight and produce a sharp bubble outline. Since it was proposed to relate the pressure variation in the gas ante-chamber to the bubble photographs, the UV recorder and high-speed camera were synchronised. Tests were carried out to establish the frequency response of the pressure measurement system and the phase shift caused by the presence of the tube linking the pressure tapping to the pressure transducer. The total time taken for the pressure wave to travel from the orifice to the transducer was found to be two milliseconds.

In order to establish conclusively the point of bubble departure on the gas ante-chamber pressure trace, the bubble formation was photographed, with the oscilloscope trace of the pressure transducer output superimposed on the image, using a twin lens 16 mm Hitachi high-speed camera.

Tests were carried out in which high-speed photographs and gas ante-chamber pressure traces were obtained for a range of air mass flow rates through four different orifice sizes from 1.586 to 3.034 mm diameter. The highest air mass flow rate for each orifice was dictated by the upper level of stable bubble formation. The tests were conducted for temperature differences of 0 °C, 30 °C and 47 °C between the air and water. The bubble outline, enlarged thirty times, was projected onto a graduated screen. The bubble volume was determined from this outline, assuming three dimensional symmetry, by dividing the shape into a series of truncated cones.

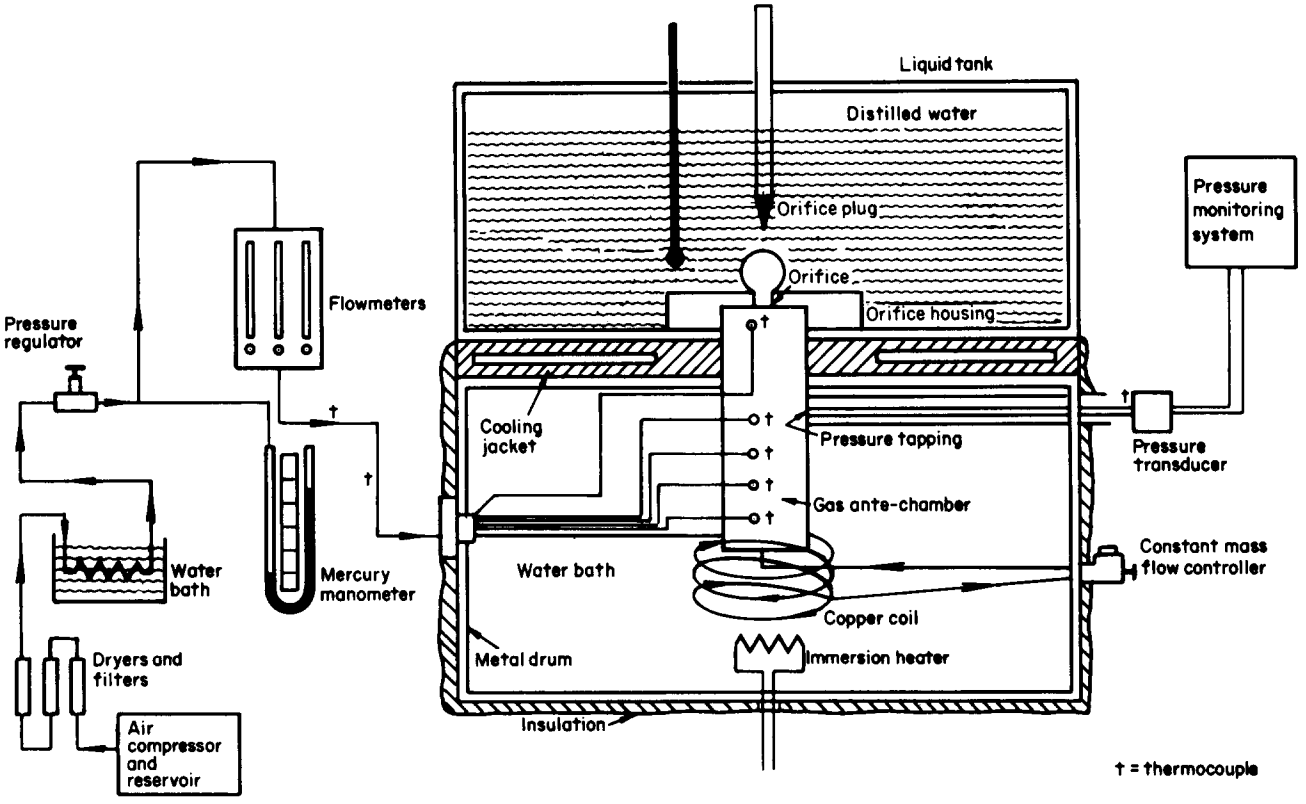

Fig 2 Apparatus to study the bubble formation process

Values for the bubble frequency were obtained from the trace produced by the UV recorder.

Results and discussion

Isothermal bubble formation

A typical trace of the gas ante-chamber pressure measured differentially with respect to a fixed datum is shown in Fig 3, for one test. The related events during the bubble formation are shown in Fig 4.

As a result of the detailed investigation using both types of high-speed camera, it was found that bubble departure from the orifice occurred at the point of minimum gas ante-chamber pressure for the majority of the tests. At the highest gas mass flow rates the point of bubble departure took place about one or two milliseconds earlier than this. The high-speed photographs of these cases indicated that when the bubble departed, the residual bubble left at the orifice continued to expand due to the existence of a low pressure region in the wake of the departing bubble, and thus the pressure in the gas ante-chamber continued to fall.

The linear increase of gas ante-chamber pressure following departure occurred as a result of the fixed inflow of gas into the ante-chamber, without any significant displacement of the bubble envelope taking place. Bubble growth then caused the ante-chamber pressure to fall once again, the point of inflexion being associated with the change from the purely radial movement of the bubble envelope during the growing stage to the coupled radial and translatory movement of the elongating stage.

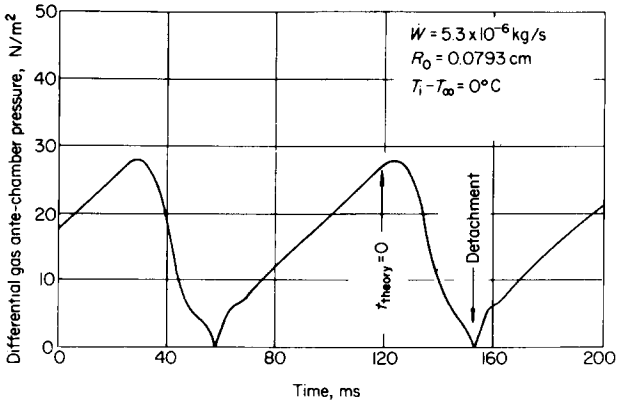

Fig 3 Time variation of gas ante-chamber pressure (isothermal)

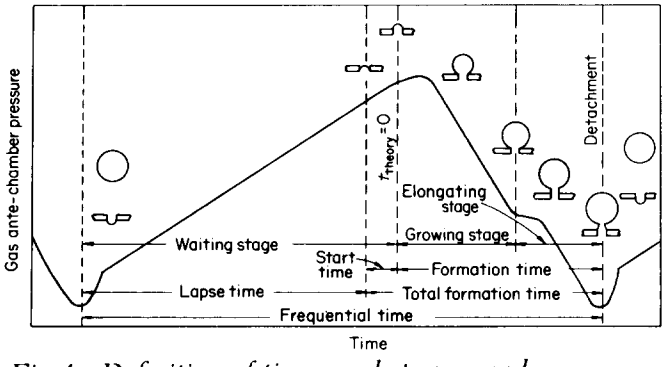

Fig 4 Definition of times and stages used

The variation of the mass flow rate of gas into the bubble during the formation period was obtained from the recorded pressure trace using Eq (3), and is shown in Fig 5 for one test condition. The point of transition between the growing stage and elongation stage, given by the solution of Eq (16), was found to be in good agreement with the experimentally observed values for all tests, and occurred at the point of maximum mass flow rate into the bubble.

The variation of frequency of bubble formation, obtained directly from the traces of the gas ante-chamber pressure over a large number of bubble formation periods, is shown in Fig 6 for two of the four orifices tested. The three main regimes of stable bubble formation were observed in which the bubble formation period remained stable over a long period of time.

The transition between the regimes for constant volume and slowly increasing volume gave rise to a regime where two bubbles of different sizes were alternately formed at the orifice. Once the cyclic process had settled down, the frequential time for each of the two types was virtually constant (Fig 7), and each of the measured frequencies so obtained is shown joined by a vertical line in Fig 6. It was observed that during this dual type of bubble formation, the first bubble grew to a final spherical shape (type A), and after detachment, the pressure in the liquid behind the departing bubble was sufficiently lower than the gas ante-chamber pressure to allow the rapid formation of a long cylindrical bubble (type B). After the departure of this bubble there was a long pause to allow the build up of pressure in the ante-chamber necessary to form the spherical bubble.

The measurements of bubble volume, obtained from an analysis of the high-speed films for the bubble formation period up to the point of departure, are shown in Fig 8. These gave consistent results, and the final bubble volumes at departure, obtained from this procedure, were checked against the final volumes found by dividing the gas flow rate by the bubble frequency measured on the UV traces, in order to substantiate the validity of the photographic measurements. Agreement was normally within 1%.

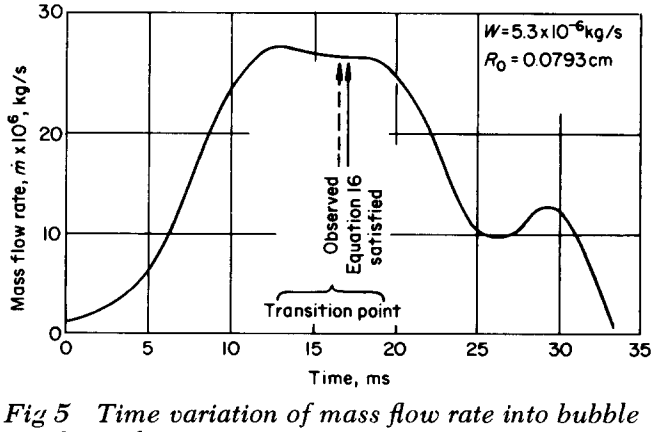

Fig 5 Time variation of mass flow rate into bubble (isothermal)

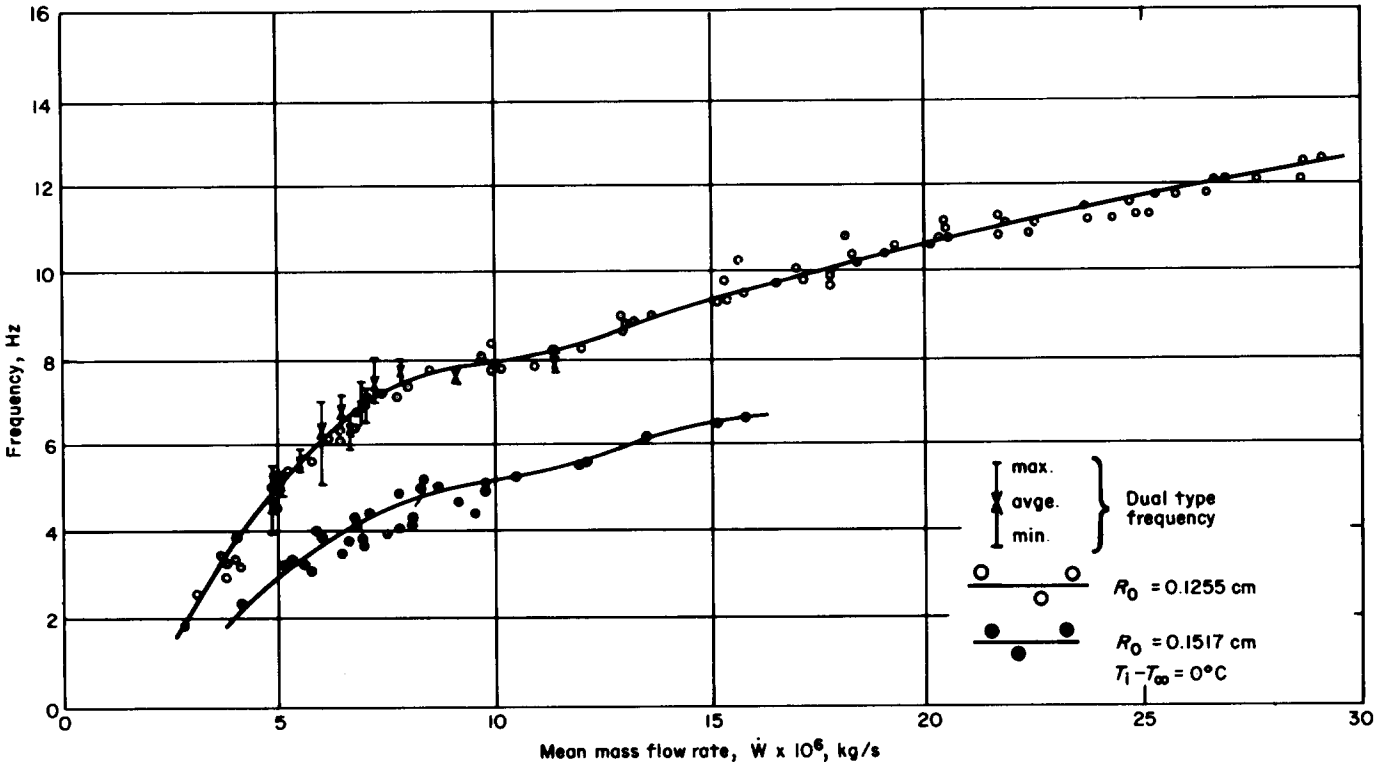

Fig 6 Variation of bubble frequency with mean mass flow rate (isothermal)

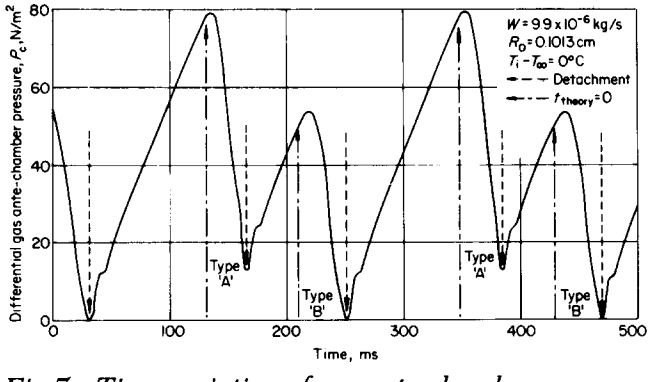

Fig 7 Time variation of gas ante-chamber pressure for regular dual type bubble formation (isothermal)

The variation of bubble volume with time obtained from the theoretical analysis is also shown in Fig 8. The predicted bubble volume was in good agreement with the measured value over the complete bubble formation period. The maximum difference between the experimental and predicted terminal bubble volume was found to be within 7% for all tests.

Bubble formation with heat transfer

In general, it was found that the effect of heat transfer caused the bubble formation process to be less regular and stable than in the isothermal case. In addition, as the temperature difference was increased, the range of mean mass flow rates where regular, stable formation could be maintained was decreased. Bubble formation was particularly susceptible to any disturbances occurring during the first few milliseconds of growth. In the case of heat transfer,

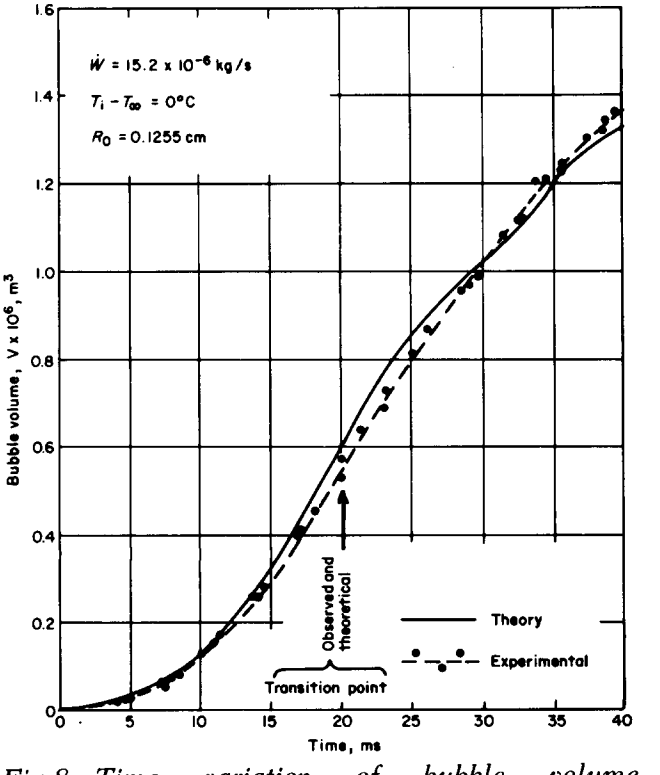

Fig 8 Time variation of bubble volume (isothermal)

minor variations in the thermal boundary layer were possible at this early stage which arose from the disturbance of the liquid caused by the departure of the preceding bubble. In fact, the system was not sufficiently stable to consistently reproduce the dual type of bubble formation which was observed in the isothermal study. It was found that no regular, stable,

bubble formation could be maintained for the orifice of diameter 3.034 mm whatever mean mass flow rate was used. Curves of bubble frequency are shown in Fig 9 for a temperature difference of 30 °C. Compared with the isothermal case, heat transfer seriously curtailed stable bubble formation in the lower mass flow rate region.

Heat transfer appeared to have very little effect on the gas ante-chamber pressure traces with the point of transition, and bubble departure remaining unaltered. This was to be expected since these were governed by the hydrodynamics of the system.

The variation of bubble volume with time for the diabatic case is shown in Fig 10, together with the isothermal results and the theoretical prediction based on Eq (31). A study of all the experimental data revealed that there was little difference between either the shape of the curves or the terminal bubble volumes for the isothermal and diabatic results. Once again the experimental and theoretical results were in very close agreement for both the time variation of the bubble volume and also the terminal volume at departure.

The change in temperature of the gas in the bubble, produced as an intermediate result during the numerical solution of the set of governing equations is shown in Fig 11. The temperature of the gas fell very rapidly during the initial stages of bubble growth indicating that the majority of the heat transfer took place within the first millisecond. These results were used to calculate a time-average surface heat transfer coefficient for the bubble formation period. The values for the experimental test conditions (0.8–1.8 kW m^{-2} K^{-1}) were within the range 0.5–7.5 kW m^{-2} K^{-1}, recorded experimentally during the formation of superheated steam bubbles in saturated water at elevated pressures[16]. In the case of heat transfer from the surface of a saturated steam bubble to a subcooled liquid stream[17], where mass transfer played a significant role, the measured values were far higher.

Conclusions

1. This theoretical solution for the bubble formation process was found to give very good agreement with the experimental results for the time variation of the bubble volume for both stages of the bubble formation, with and without heat transfer, over a wide range of gas mass flow rates and orifice sizes. In addition, the transition point between the two stages was predicted accurately.

2. From the experimental investigation it was found that heat transfer had only a minor effect on the bubble formation process, mainly by reducing the stability and the range of operation for a given orifice.

3. From the results of the theoretical solution of the bubble formation process it was found that the vast majority of the heat transfer between the growing bubble and the liquid occurred in the first few instants of bubble formation.

4. Time-average values for the surface heat transfer coefficient were predicted in the range 0.8–1.8 kW m^{-2} K^{-1}.

Acknowledgement

The authors wish to thank the Ministry of Defence and the Science Research Council for their financial support.

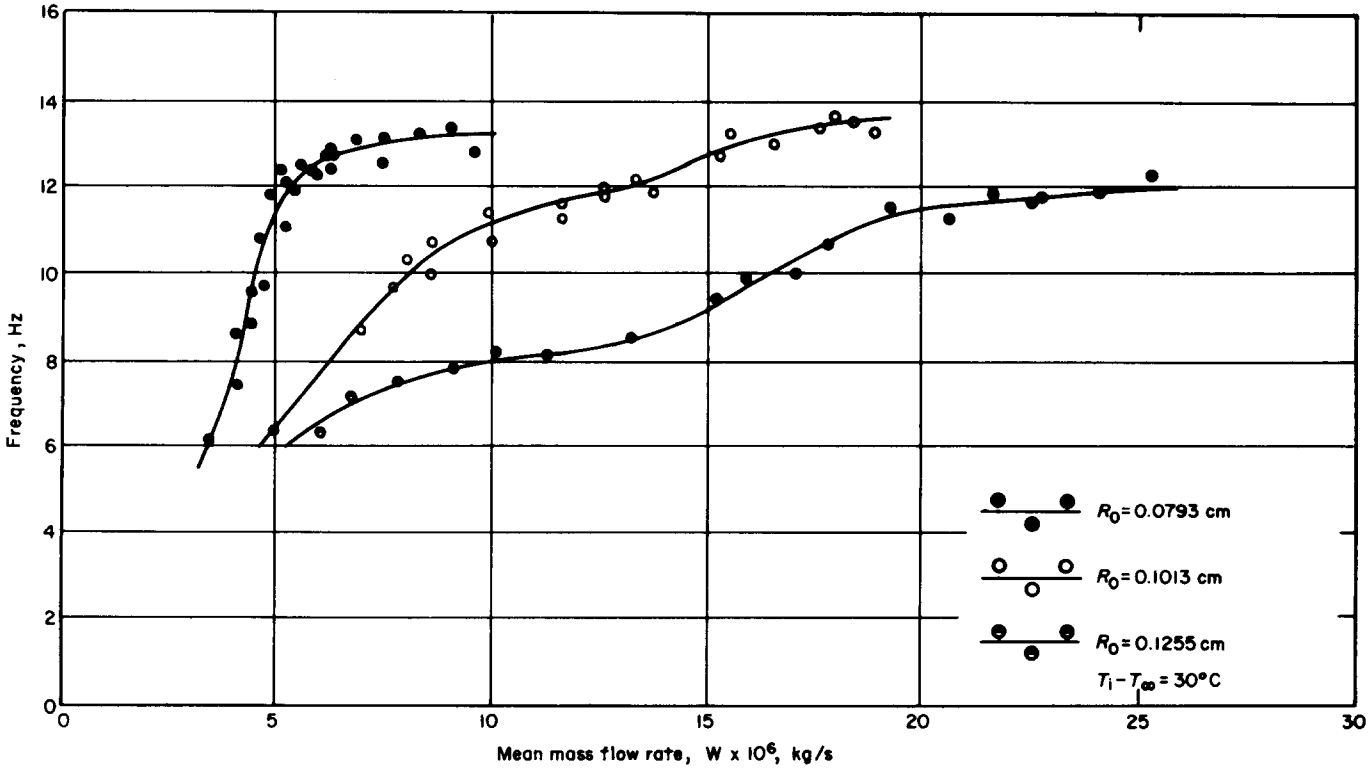

Fig 9 Variation of bubble frequency with mean mass flow rate (non-isothermal)

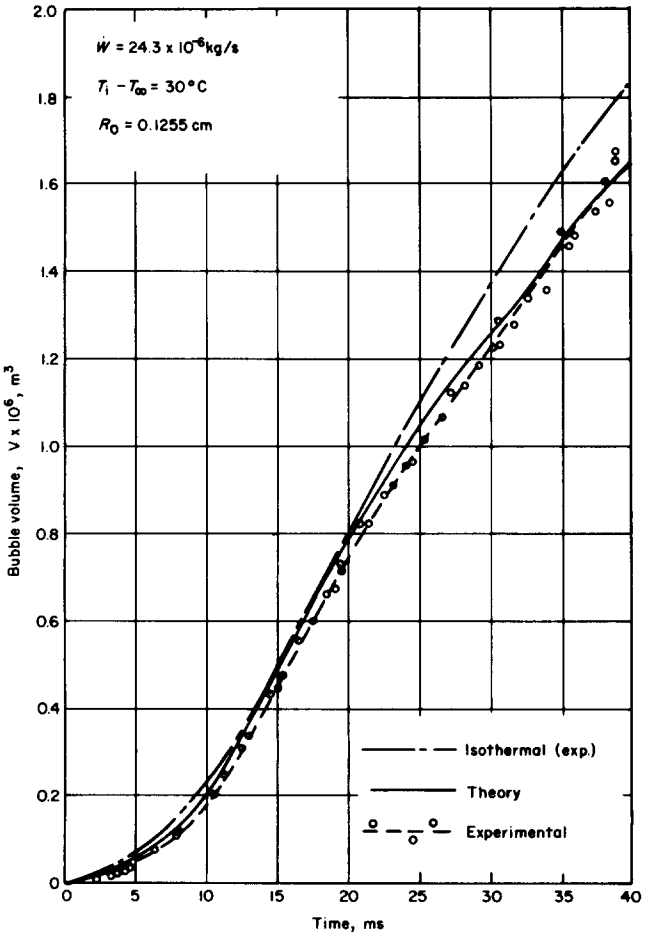

Fig 10 Time variation of bubble volume (non-isothermal)

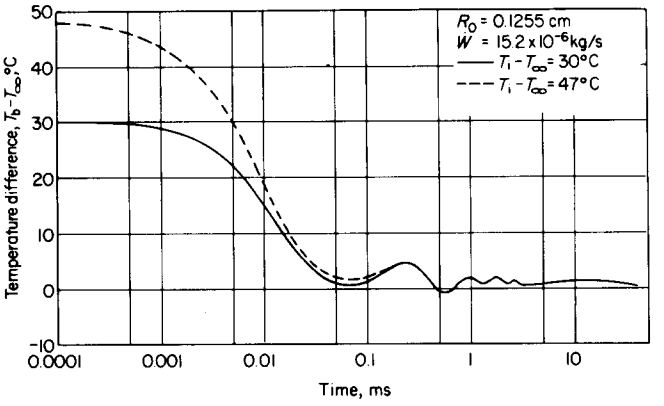

Fig 11 Time variation of bubble temperature

References

1. **Hughes R. R., Handlos A. E., Evans H. D. and Maycock R. L.** The formation of bubbles at simple orifices. *Chem. Eng. Progress, 1955,* **51**, *557–563*
2. **Davidson J. F. and Schuler B. O. G.** Bubble formation at an orifice in a viscous liquid. *Trans. Inst. Chem. Engrs, 1960,* **38**, *144–154*
3. **Hayes W. B., Hardy B. W. and Holland C. D.** Formation of gas bubbles at submerged orifices. *A.I.Ch.E.J., 1959,* **5**, *319–324*
4. **Sullivan S. L. Jnr., Hardy B. W. and Holland C. D.** Formation of air bubbles at orifices submerged beneath liquids. *A.I.Ch.E.J., 1964,* **10**, *848–854*
5. **Kupferberg A. and Jameson G. J.** Bubble formation at a submerged orifice above a gas chamber of finite volume. *Trans. Inst. Chem. Engrs, 1969,* **47**, *241–250*
6. **McCann D. J. and Prince R. G.** Bubble formation and weeping at a submerged orifice. *Chem. Eng. Sci., 1969,* **24**, *801–814*
7. **Witze C. P., Schrock V. E. and Chambre P. L.** Flow about a growing sphere in contact with a plane surface. *Int. J. Heat and Mass Transfer 1968,* **11**, *1637–1652*
8. **Kotake S.** On the mechanism of nucleate boiling. *Int. J. Heat and Mass Transfer, 1966,* **9**, *711–728*
9. **L'Ecuyer M. R. and Murphy S. N. B.** Energy transfer from a liquid to gas bubbles forming at a submerged orifice. *NASA TND-2547, Purdue University, 1965*
10. **Haynes J. B.** Heat transfer during bubble formation. *Ph.D. Thesis. The City University, Sept. 1977*
11. **Poritsky H.** The growth or collapse of a spherical bubble or cavity in a viscous fluid. *A.S.M.E. 1952, 313–321*
12. **Levich V. G.** Physicochemical Hydrodynamics. *Prentice-Hall, 1962, 378*
13. **Haynes J. B.** Theory for the formation and rise of single air bubbles in isothermal and non-isothermal liquids. *The City University, Research Memorandum ML68, May 1974*
14. **Wraith A. E. and Kakutani T.** The pressure beneath a rowing rising bubble. *Chem. Eng. Sci., 1974,* **29**, *1–12*
15. **Ruckenskein E. and Davies E. J.** The effects of bubble translation on vapour bubble growth in a superheated liquid. *Int. J. Heat and Mass Transfer, 1971,* **14**
16. **Schmidt H.** Bubble formation and heat transfer during dispersion of superheated steam in saturated water—II. *Int. J. Heat and Mass Transfer, 1977,* **20**
17. **Bankoff S. G. and Mason J. P.** Heat Transfer from the surface of a steam bubble in turbulent subcooled liquid stream. *A.I.Ch.E., March 1962,* **8***(1)*